DESIGN AND TESTING OF A MICROCHANNEL HEAT EXCHANGER WORKING AS CONDENSER AND EVAPORATOR

Emanuele Zanetti[(a)], Marco Azzolin[(a)]*, Stefano Bortolin[(a)], Giulio Busato[(b)], Davide Del Col[(a)]

[(a)]Department of Industrial Engineering, University of Padova
Via Venezia 1 – 35131 Padova, Italy

[(b)]Hiref SpA
Viale Spagna, 35020, Tribano, Padova, Italy

* Corresponding Author
Tel.: +39 049 8276885; Fax: +39 049 8276896; Email: marco.azzolin@unipd.it

ABSTRACT

In the recent years, international agreements and regulations push for a reduction of production and utilization of Hydrofluorocarbons (HFCs), while achieving high efficiency remains a crucial aspect for refrigeration and air conditioning systems. One of the possible candidates to replace the high global warming potential (GWP) fluid currently employed in heat pump systems (R410A) is the refrigerant R32, which belongs to A2L class. In addition to adopting low-GWP refrigerants, charge minimization is a major design objective for such systems, mainly in the case of flammable refrigerants. In the case of reversible heat pumps, a reduced volume of the heat exchangers limits the refrigerant charge migration between condenser and evaporator when switching between the operation modes. The refrigerant charge minimization coupled with the use of new refrigerants can therefore be considered one of the most important objectives for new heat pump developments. The microchannel technology helps for this purpose. The present paper presents an air-to-refrigerant microchannel heat exchanger working with R32, realized in the framework of the European Project GEOTeCH. The prototype heat exchanger, working both as the condenser and as the evaporator, has been tested on a dual source (air and ground) heat pump, which can operate in heating and cooling modes. A model of the microchannel heat exchanger has also been developed and the predicted performance have been compared with the experimental measurements. In the end, the model has been used to estimate the refrigerant charge trapped in the minichannel when it works as the condenser and the results have been compared with those obtained using a traditional finned coil heat exchanger.

1. INTRODUCTION

The reduction of anthropogenic greenhouse gases (GHG) emissions is a key target to mitigate the climate change. The contribute of energy consumption to climate change is significant and a remarkable portion is related to the HVAC and the refrigeration industry since, as reported by Irudaya Raj *et al*. (2017), HVAC systems represent one-fifth of the total electrical power consumption. The improvements of new technologies and the correct design of innovative systems such as multisource heat pumps can lead to a reduction of energy consumptions. However, the refrigerants actually adopted are most of the time high global warming potential (GWP) fluids. Recently some actions have been undertaken to reduce or prohibit the use of high GWP fluids, i.e. the European Union with the Regulation No 517/2014, and fluids with low GWP claim their role in the HVAC and refrigeration industry. As reported by Mota-Babiloni *et al*. (2017), R32 can be a good alternative for air-conditioning and heat pump systems. The refrigerant R32 has a GWP equal to 677 (70 % lower than that of R410A) and it is classified as mildly flammable by ASHRAE Standard 34 (2013). Thus, charge reduction is a key target for systems working with R32.
The present study focuses on the use of a microchannel heat exchanger (MCHX) as condenser and evaporator in a dual source heat pump working with R32. Microchannel heat exchanger technology allows to realize compact devices with a reduction of the refrigerant charge. Del Col *et al*. (2010) investigated a shell-and-tube microchannel heat exchanger. Other studies were focused on air-to-refrigerant microchannels heat exchangers for heat pump

systems showing their positive effect on refrigerant charge reduction. Park and Hrnjak (2008) compared a round-tube-plate-fin (RTPF) heat exchanger (HX) and a MCHX with approximately the same volume and fin pitch working as condensers in an air conditioning system using R410A. Neglecting an economical evaluation, they found an increase of the COP equal to 13.1 % by using the MCHX and a 9.2 % charge reduction. Illan Gomez *et al*. (2017) compared a minichannel heat exchanger and a conventional fin and tube heat exchanger working as condensers for a residential air-to-water chiller using R134a; in most of the tested and simulated cases, the charge reduction by using the microchannel heat exchanger was up to 21% and the performance were slightly worse. They also found that the subcooling is the key parameter for having a strong charge reduction.
Nevertheless, there are only few works regarding the use of microchannel heat exchangers as evaporators in air-conditioning and heat pump systems. The main issue of these configuration is the refrigerant two phase distribution, that can lead to a 20% performance reduction (Kulkarni *et al*. 2004). Garcia-Cascales *et al*. (2016) studied the performance of a reversible heat pump working with R134a comparing two different air-to-refrigerant evaporators: a microchannel heat exchanger and a round tube plate fin (RTPF) heat exchanger. The charge reduction obtained in the evaporator was up to 11.7% when working with the MCHX but the COP decreased by 4% compared to that of the RTPF. They concluded that the use of MCHX evaporator in a heat pump deserves further studies.
In the present paper, a MCHX is presented and tested in a heat pump prototype. The performance of the MCHX are compared to those of a conventional RTPF-HX. A model of the MCHX has been developed and tested against the experimental data to have a reliable tool for the design of these systems.

2. HEAT PUMP PROTOTYPE

The present prototype is a heat pump for heating, cooling and domestic hot water (DHW) production working with both ground and air as source/sink. This heat pump prototype has been developed within the European project GEOTeCH (Geothermal technology for economic cooling and heating) in the framework of Horizon 2020 research and innovation program. Table 1 shows all the possible operative conditions of the heat pump divided in two main categories: summer (production of chilled water or DHW production) and winter (production of hot water for heating system or DHW production). For each operation mode, the secondary fluid at the condenser and evaporator is specified. For example, in mode "1 MCHX-SUMMER" the heat pump produced chilled water and the air-to-refrigerant microchannel heat exchanger (MCHX) is used as condenser. Experimental tests on this prototype have been conducted under controlled conditions in the climatic chamber at the R&D Laboratory of Hiref Spa and in the present paper only the working condition in air mode will be presented and analyzed.

Table 1: Operative conditions of the heat pump.

Mode	SUMMER		Mode	WINTER	
	Condenser	Evaporator		Condenser	Evaporator
1 RTPF-SUMMER	AIR	USER (chilled water)	6 RTPF-WINTER	USER (water for heating system)	AIR
1 MCHX-SUMMER	AIR	USER (chilled water)	6 MCHX-WINTER	USER (water for heating system)	AIR
2 SUMMER	GROUND	USER (chilled water)	7 WINTER	USER (water for heating system)	GROUND
3 SUMMER	DHW	USER (chilled water)	8 WINTER	DHW	GROUND
4 RTPF-SUMMER	DHW	AIR	9 RTPF-WINTER	DHW	AIR
4 MCHX-SUMMER	DHW	AIR	9 MCHX-WINTER	DHW	AIR
5 SUMMER	DHW	GROUND			

2.1 Experimental set up

The system layout of the heat pump is shown in Figure 1: the blue line represents the refrigerant circuit when working in summer-air conditions (production of chilled water), the red line is for the winter-air mode (production of water for the heating system) and the black lines represent the water circuit. Solenoid valves (labelled in Figure 1 with an "S") allow to change between different operative modes. Referring to Figure 1: the scroll compressor equipped with an inverter is numbered with 1, 2 is the refrigerant-to-water brazed plate heat exchanger, 3 is the liquid receiver, 4 is the electronic expansion valve (EEV), 5 is the air-to-refrigerant heat exchanger and 6 is the variable speed drive water pump.

The present experimental tests have been conducted in air mode, using alternatively two different types of air-to-refrigerant heat exchangers working as evaporator or condenser: a standard RTPF-HX and a MCHX. A brazed plate heat exchanger BPHX (labelled 2) is dedicated for the user on the water side. In summer-air mode, the valve S3 is open and after the compressor, the refrigerant condenses in the air-to-refrigerant heat exchanger and then it is sent through the liquid receiver to the expansion valve before evaporating in the user BPHE (2); then the fluid goes back to the compressor through the valve S1. In winter-air mode, solenoid valves S2, S6 and S4 are open: the refrigerant, exiting the compressor, condenses in the user BPHX (2), expands in the EEV and then evaporates in the air-to-refrigerant heat exchanger. Considering the secondary fluid side, the water temperature at the inlet of the BPHX is controlled using the laboratory facility while its flow rate is regulated by a variable speed water pump. The air temperature and the relative humidity are controlled inside the climatic chamber.

In Figure 1, the locations of the measuring sensors are also displayed. In the refrigerant circuit (R32), the pressure is measured by pressure transducers installed at compressor suction/discharge, at condenser outlet (air heat exchanger in winter mode and BPHX in summer mode) and after the expansion valve. The temperatures are measured with T-Type thermocouples at compressor suction/discharge, at condenser outlet and after the liquid receiver. On the secondary water circuits, temperature measurements are performed with resistance thermometers (PT-100) at the inlet and outlet of the BPHXs. Pressure drop on the water side and volumetric water flow rate are measured with differential pressure transducers and electromagnetic flow meters respectively. On the air side, the pressure drop is measured with a differential pressure transducer and T-Type thermocouples are used to measure the inlet/outlet temperatures.

The electrical power consumptions are also measured for compressor and auxiliaries.

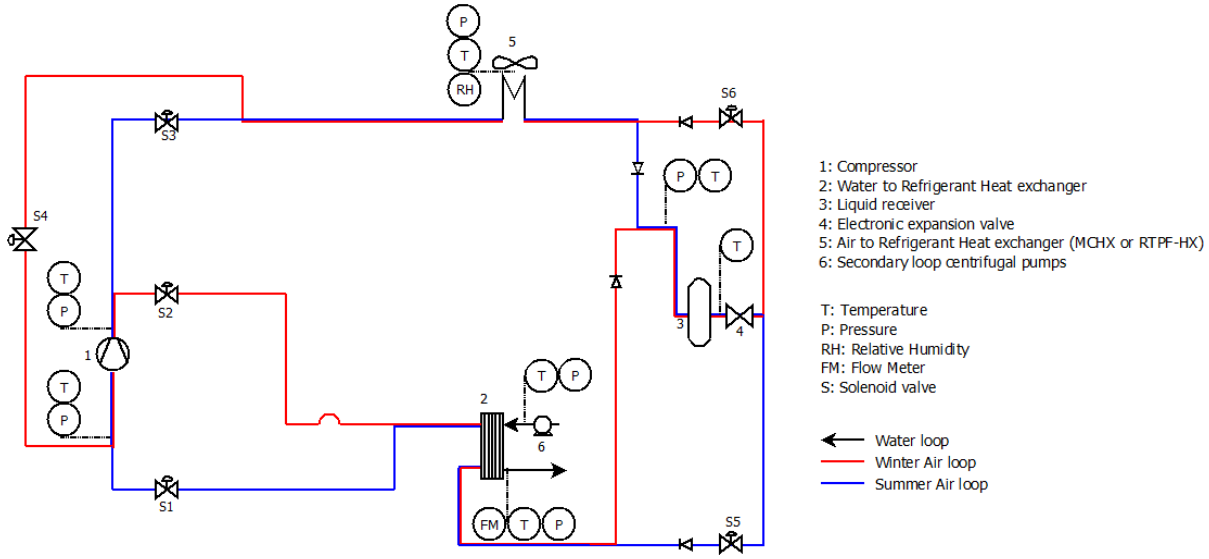

Figure 1: Layout of the heat pump prototype during tests. Blue lines represent the refrigerant circuitry for the summer-air mode, red lines for the winter-air mode. Black lines represent the water circuit. Additional heat exchangers are not reported here.

2.2 Air-to-Refrigerant Heat Exchanger

The present heat pump can use alternatively two different air-to-refrigerant heat exchangers: a round tube plain fin heat exchanger (RTPF-HX, Figure 2a) or a microchannel heat exchanger (MCHX, Figure 2b). The RTPF heat exchanger has 9 circuits and 3 rows (45 tubes for each row). The internal diameter of the tubes is equal to 8 mm. The MCHX has been fabricated starting from two commercially available MCHXs connected in series. As it can be

seen in Fig. 2b, the resulting configuration consists of a 2 ranks heat exchanger with 75 aluminum multiport tubes (vertically oriented) for each rank. The frontal area of the MCHX is approximately the same of that of the RTPF-HX. When working as evaporator, the refrigerant flows in upward direction inside each rank whereas it goes in downward direction when working as condenser. It must be mentioned that the air-to-refrigerant heat exchanger is in co-current configuration when working as condenser, while it is in counter-current when working as evaporator.

a) b)

Figure 2: Pictures of the heat pump prototype working with the RTPF-HX (a) and with the MCHX (b).

2.3 Data Reduction

Experimental tests have been conducted in winter-air and summer-air modes, using the air-to-refrigerant heat exchanger respectively as evaporator or condenser. Data have been recorded during steady-state conditions (50 measurements taken every 5 seconds). The refrigerant mass flow rate is not directly measured but it is estimated performing an energy balance on the water side at the BPHX. The heat flow rate at the BPHX is:

$$Q_{BPHX} = \rho_w \cdot \dot{V}_w \cdot c_w \cdot |\Delta T_w| \tag{1}$$

where $\dot{V}_w$ is the volumetric water flow rate, ρ_w is the water density, c_w is the specific heat evaluated at the mean water temperature and ΔT_w is the water temperature difference between inlet and outlet. In winter-air mode, the BPHX works as condenser: the refrigerant enthalpy at the inlet of the condenser is assumed equal to that at the outlet of the compressor and evaluated using Refprop (Lemmon *et al.*, 2013) from the temperature and pressure measurements; the refrigerant enthalpy at the outlet of the condenser is calculated from the temperature and the pressure since the fluid is subcooled. In summer-air mode the BPHX works as evaporator: the outlet refrigerant enthalpy is evaluated from the temperature and pressure measurements since the fluid is superheated; the enthalpy at the inlet is evaluated from the pressure measurement and using the same enthalpy at the liquid receiver, which is determined from the measured temperature and pressure. Thus, the refrigerant mass flow rate can be calculated in summer-air mode with Eq. 2 and in winter-air mode with Eq. 3

$$\dot{m}_{ref} = \frac{Q_{BPHX}}{h_{out_{evap}} - h_{in_{evap}}} \tag{2}$$

$$\dot{m}_{ref} = \frac{Q_{BPHX}}{h_{in_{cond}} - h_{out_{cond}}} \tag{3}$$

3. EXPERIMENTAL RESULTS

The experimental tested conditions are summarized in Table 2. Each test has been realized both using the RTPF-HX and the MCHX heat exchanger. Tests have been conducted changing the compressor speed (the scroll compressor is driven by inverter) and the fan speed. During the tests, the water temperature difference in the BPHX has been maintained at about 5 K (45 °C - 50 °C in winter tests and 12 °C - 7 °C in summer tests) by varying the pump velocity. Subcooling and superheating were set and kept constant at 1 K at 6 K respectively.

Table 2: Experimental tested conditions.

MODE	COMPRESSOR (Hz)	FAN INPUT (%)	WATER TEMP. (°C)	SUB-COOLING/ SUPER-HEATING (K)
1 Summer-Air	50	50	12 to 7	1
2 Summer-Air	50	70	12 to 7	1
3 Winter-Air	50	50	45 to 50	6
4 Winter-Air	70	70	45 to 50	6

Figure 3a shows the values of the condensation temperature, determined from the pressure measured at the inlet of the air-to-refrigerant heat exchangers in summer-air mode (conditions 1 and 2 of Table 2). When the fan is working at 50% of the voltage signal input, the condensation temperature is 1 K lower when the MCHX is installed (the air temperature remains the same in both cases). This means that, under these conditions, the MCHX performs better than the standard RTPF-HX. When the fan input is fixed at 70% of the maximum, the measured air temperature is equal to 29.9 °C for the RTPF-HX and equal to 30.9 °C for the MCHX; the condensation temperature in the two cases is approximately the same. Figure 3a also shows the effect of the fan velocity on the performance of the heat exchangers: at the same compressor frequency, when increasing the fan voltage, the condensation temperature decreases showing the benefits of increasing the air velocity and thus the air-side heat transfer coefficient.
Experimental results of the heat pump working in winter-air conditions are shown in Figure 3b. Measurements have been recorded at different fan velocity (50% and 70%) and two compressor velocities (50 Hz and 70 Hz). When the fan input is at 50%, the compressor works at 50 Hz frequency and the air temperature is around 14.5 °C for both the tests with MCHX and RTPF-HX. The evaporation temperature is nearly the same but the MCHX presents lower air-side pressure drop (18 Pa) compared with the RTPF-HX (28 Pa). When working at 70% fan input and with the compressor at 70 Hz, the air temperature is equal to 15.4 °C in the case of the RTPF-HX and to 14.6 °C in the case of the MCHX. The evaporation temperature reflects the air side temperature difference between the two tests showing a lower saturation temperature for the MCHX (equal to 1.7 °C) compared to that of the RTPF-HX (equal to 2.4 °C) and therefore the two devices present a similar heat transfer performance. It must be mentioned that the air-side pressure drop for the MCHX and for the RTPF-HX is respectively equal to 35 Pa and 52 Pa.

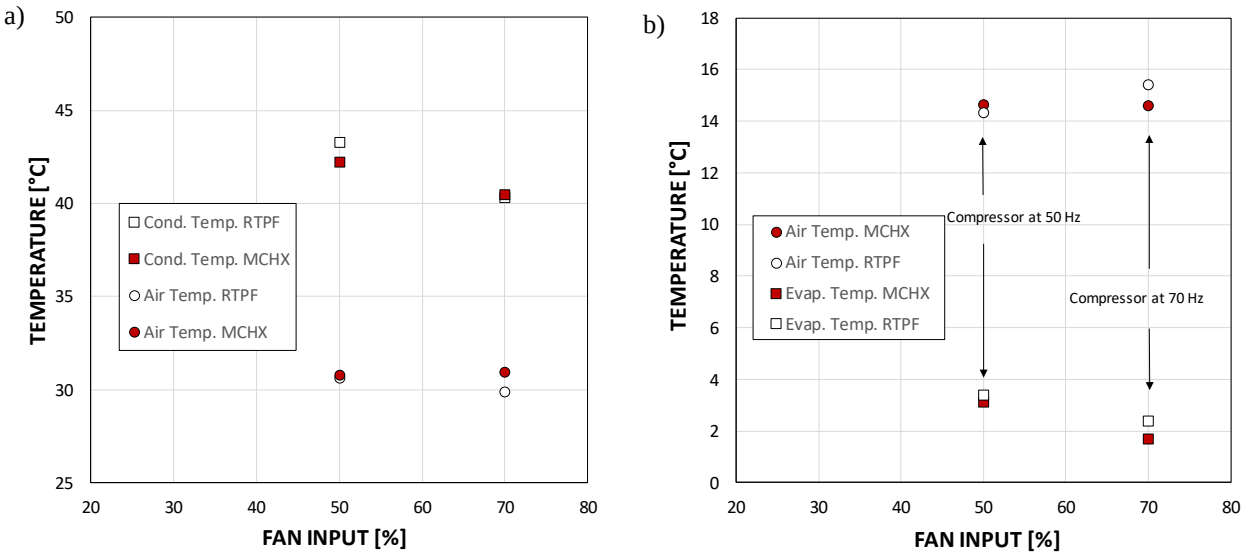

Figure 3: Comparison between the RTPF-HX and the MCHX (a) in summer air-mode at variable fan speed and fixed compressor frequency (50 Hz) and (b) in winter air mode at variable fan speed and variable compressor frequency (50 Hz when fan is at 50% and 70 Hz when fan is at 70%)

During the experimental tests an infrared (IR) camera was used to analyze the refrigerant distribution inside the MCHX. Since the MCHX is in counter-flow when working as evaporator and in co-current flow when working as condenser, the thermography refers to condenser inlet and evaporator outlet. Figure 4a shows that during

condensation (fan at 70% and compressor at 50 Hz) the refrigerant is equally distributed between the parallel channels; the desuperheating is limited to the entrance part of each tube. Figure 4b displays the IR image of the MCHX working in winter conditions (as evaporator) with the compressor at 50 Hz and 50% of fan input. In this case, the image refers to the second rank of the heat exchanger, where the fluid is superheated: two wide areas at high temperature (area in red in Figure 4b) can be detected, separated by a central lower temperature region. This means that the refrigerant mass flow rate is not equally distributed in all the parallel channels of the MCHX and this phenomenon can lead to a reduction of the achievable performance of the heat exchanger.

a) b)

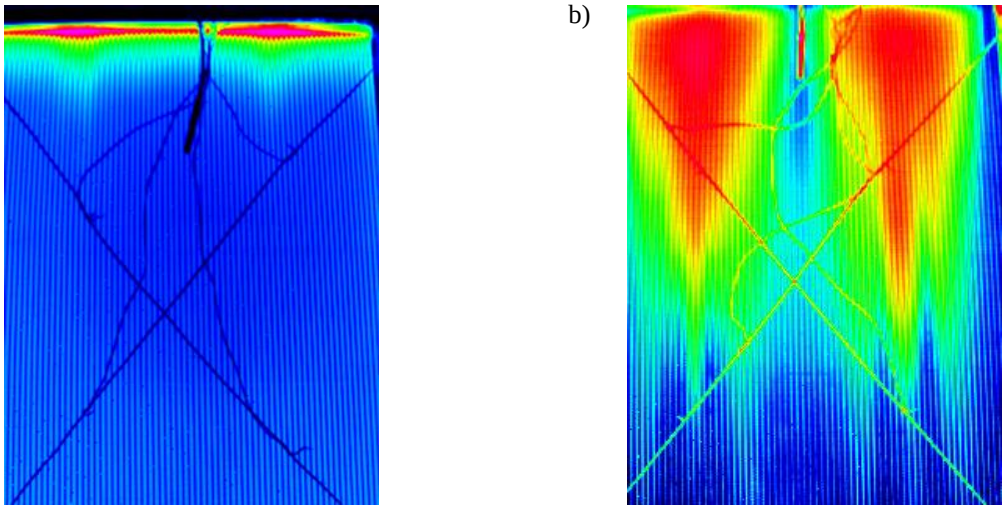

Figure 4: IR camera images of the MCHX taken during the experimental tests: a) working as condenser (fan at 50% and compressor at 70 Hz); b) working as evaporator (fan at 50% and compressor at 50 Hz).

4. SIMULATION MODEL

4.1 Mathematical model

A mathematical model has been developed, in Matlab® environment to design and predict the functioning of an air-to-refrigerant microchannel heat exchanger (i.e. calculate the heat flow rate exchanged and outlet conditions of the fluids knowing the inlet thermodynamic conditions and the flowrates). Otherwise, it is possible, with an iterative procedure, to estimate the evaporation and condensation temperature that are needed to obtain an imposed value of vapor superheating or liquid subcooling.

The model has been implemented by dividing the volume of the heat exchanger in macro-elements: ranks, collectors and tubes. The collectors, which have been considered adiabatic, have been discretized considering a number of elements equals to the number of tubes per rank. Each single tube has also been divided in discrete elements, where the mass, energy and momentum equations are solved for each fluid: this approach allows to consider every element as an independent heat exchanger, where the inlet conditions are equal to the outlet conditions of the previous element. For the tube elements, the outlet conditions of the fluids are calculated with the ε-NTU method, until the end of the heat exchanger length.

The Number of Transfer Units (NTU) depends on the UA product, where A is the heat transfer area and U the global heat transfer coefficient:

$$UA = \frac{1}{R_{ref} + R_c + R_{air}} \tag{4}$$

In Equation (4) R_{ref} and R_{air} are the convective thermal resistances on the refrigerant and air side, R_c is the conduction resistance of the aluminum wall. The heat transfer coefficients are calculated with the correlations described in the next section and they are related to the mean thermo-physical properties of the fluids between inlet and outlet of each element. The model has been developed to manage different type of geometries, i.e. changing number of ranks, number of passes, number of multiport channels, configuration (co-current or counter-current).

4.2 Simulation of air and refrigerant flow

The present model uses different correlations to predict the air and refrigerant heat transfer coefficients. Regarding multiport MCHXs with louvered fins, there are several works in the literature dealing with the determination of the air heat transfer coefficient and friction factor. The majority of correlations predict the value of the Colbourn number j and friction factor f using a Reynolds number that depends on the louver pitch Lp, as the Davenport (1983) correlation or the Wang *et al.* (2000) correlation. The MCHX here investigated presents smooth (non-louvered) triangular fins and therefore the heat transfer coefficient and the friction factor are calculated following the description of Muzychka and Yovanovich (2004). The procedure proposed by Threlkeld *et al*. (1998) has been implemented in the model of the MCHX to consider the possibility to have air dehumidification when the MCHX works as evaporator.

On the refrigerant side, the heat transfer coefficient during vaporization has been calculated with the Lazarek and Black (1982) correlation, which was shown by Del Col *et al*. (2013) to predict with good accuracy experimental data of R32 in a microchannel with internal diameter equal to 1 mm. The condensation heat transfer coefficient has been evaluated with the Cavallini *et al*. (2006) correlation, which has been suggested even for small diameter channels (Del Col *et al*. 2015, Matkovic *et al*. 2009).

For the calculation of the two-phase pressure drop inside the microchannels the correlation developed by Del Col *et al*. (2015) has been selected. For the single-phase flow, Churchill (1977) equation has been implemented for the friction factor and Dittus-Boelter equation for the heat transfer coefficient evaluation.

The present model can also consider for a non-uniform distribution of the refrigerant inside channels, in accordance with the work of Kim and Byun (2013). Unfortunately, correlations for the distribution of the two-phase flow are rare and those available in the literature have been derived for geometries different from the present one. Thus, the calculations reported in this work have been done considering a uniform distribution of the refrigerant between the tubes.

5. SIMULATION RESULTS

The present model has been used to simulate the functioning of the MCHX and to calculate the condensation and evaporation temperature at the experimental conditions presented in Section 3. The inputs of the model are: air temperature, air relative humidity, refrigerant subcooling or superheating (depending if the heat exchanger is working as condenser or evaporator). In addition, the air velocity (calculated from the experimental fan input voltage, air-side measured pressure drop and the fan curves provided by the manufacturer) together with the R32 mass flow rate (calculated with Eq. 2 or 3) must be provided as input. A first tentative value for the evaporation and condensation temperature has also been set for each simulation. The number of axial discretizations was set equal to 100 for each rank (200 elements for the entire heat exchanger).

In case of summer tests, when the MCHX is working as condenser, the refrigerant distribution was considered uniform. Figure 5a shows the results of the simulation: the model is able to predict accurately the condensation temperature showing a maximum absolute error $|\Delta T|_{calc-exp}$= 0.26 K when the fan input is equal to 50%.

When the MCHX is working as evaporator, the refrigerant distribution is not equal in all the parallel channels (see Figure 4b). In this case, the effect of refrigerant maldistribution is accounted for by reducing the effective heat transfer area. From the images of the IR camera the number of tubes with a poor distribution of the refrigerant has been estimated and the heat transfer area reduced accordingly (total number of tubes reduced of 7% at 50 Hz and 14% at 70 Hz). Figure 5b shows the comparison between the calculated data from the model and the experimental data: the maximum absolute deviation is equal to 0.28 K when the compressor works at 70 Hz and fan input at 70%.

6. REFRIGERANT CHARGE EVALUATION

The heat exchanger model presented in Section 4 can be used also to estimate the refrigerant charge trapped in the MCHX using the Rohuani and Axelsson (1970) correlation (corrected as reported in Rouhani, 1978) to evaluate the void fraction. Table 3 presents a comparison between the refrigerant charge estimated inside the MCHX and inside the RTPF-HX: the estimation of the refrigerant mass trapped in the RTPF-HX has been done using a simplified model of the heat exchanger and using the same correlations for the void fraction.

The refrigerant charge estimation has been done for two working conditions in summer-air mode (reported in Table 2 as Condition 1 and Condition 2) when the air-to-refrigerant heat exchangers work as condensers, since most part of the total charge is kept in the condenser.

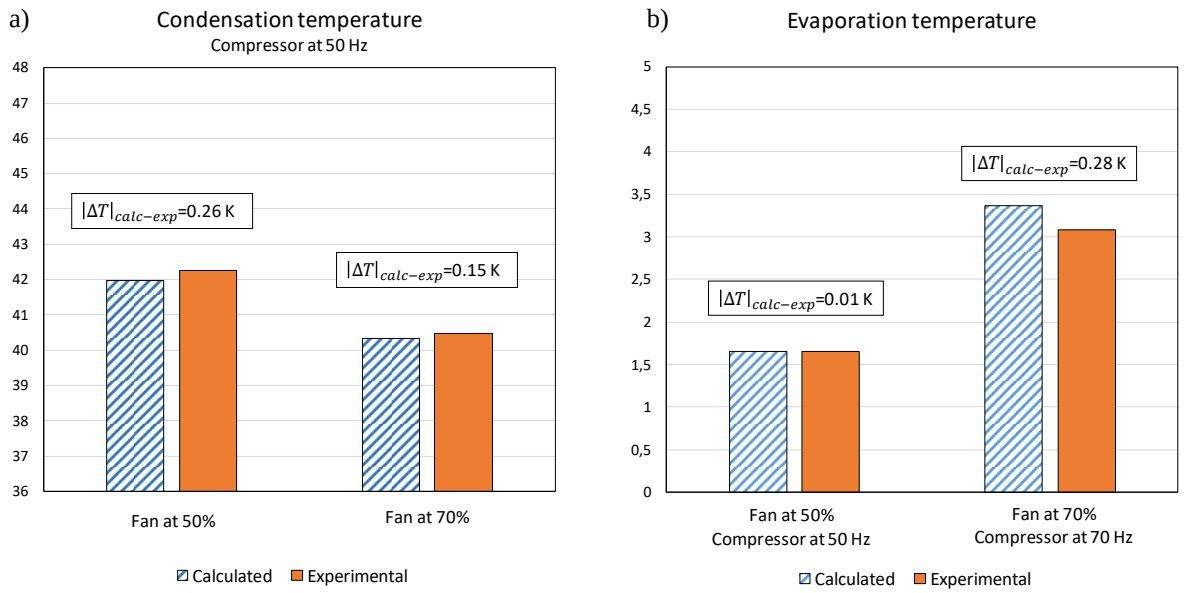

Figure 5: Comparison between experimental measurements and model results: condensation temperature in summer air mode (a) and evaporation temperature in winter air mode (b).

Table 3: Estimated refrigerant charge trapped in the tubes of the two air-to-refrigerant condensers at conditions 1 and 2 (Summer Air) of Table 2

Heat Exchanger		Unit	Refrigerant Charge	
			1 – Table 2	2 – Table 2
MCHX	First Rank	kg	0,32	0,31
	Second Rank	kg	0,96	0,95
	Total Charge	kg	1,29	1,26
RTPF-HX	Total Charge	kg	1,82	1,77
Charge reduction		%	-29,1	-28,8

7. CONCLUSIONS

In this paper, a prototype of a microchannel heat exchanger working as condenser and evaporator in a reversible dual source (ground and air) heat pump is presented. The aluminum microchannel heat exchanger has 2 ranks connected in series, 75 parallel multiport tubes for each rank and 10 microchannels per multiport tube with hydraulic diameter of about 1 mm. Experimental tests have been performed to evaluate the performance of the microchannel heat exchanger and to compare them with those of a traditional round tube plain fins heat exchanger. The frontal area of the two air-to-refrigerant heat exchangers is approximately the same since they should fit in the same heat pump framework.

The microchannel heat exchanger, at the same inlet air temperature and velocity, displays the same heat transfer performance of the round tube and plain fins heat exchanger when working as evaporator, besides it guarantees higher performance when working as condenser. Furthermore, the microchannel heat exchanger provides a reduction of the air-side pressure drop.

A numerical model of the microchannel heat exchanger has also been developed and validated using the experimental data. The maximum deviation on the estimation of the saturation temperatures was 0.26 K and 0.28 K in summer and winter mode respectively. A comparison between the charge contained inside the tubes of the two heat exchangers when working as condenser has been realized showing that it can be reduced by about 30% using the microchannel heat exchanger.

NOMENCLATURE

A	Area	(m^2)
BPHE	Brazed Plate Heat Exchanger)	(–)
c	Specific heat	$(J \cdot kg^{-1} \cdot K^{-1})$
CFD	Computational Fluid Dynamics	(–)
COP	Coefficient of performance	(–)
DHW	Domestic Hot Water	(–)
f	Friction factor	$(-)$
GWP	Global Warming Potential	(–)
GHG	Greenhouse Gases	(–)
HVAC	Heating Ventilation and Air Conditioning	(–)
HFC	Hydrofluorocarbon	(–)
HP	Heat Pump	(–)
h	Specific enthalpy	$(J \cdot kg^{-1})$
j	Colbourn number	$(-)$
$\dot{m}$	Mass flow rate	$(kg \cdot s^{-1})$
MCHX	Microchannel Heat Exchanger	(–)
R	Thermal resistance	$(K \cdot W^{-1})$
T	Temperature	(°C)
U	Global heat transfer coefficient	$(W \cdot m^{-2}K^{-1})$
$\dot{V}$	Volumetric flow rate	$(m^3 \cdot s^{-1})$
Q	Heat transfer rate	(W)
ρ	Density	$(kg \cdot m^{-3})$
ε	Efficiency	$(-)$

Subscript

air	air	in	inlet
c	conduction	max	maximum
calc	calculated	out	outlet
cond	condensation	ref	refrigerant
evap	evaporation	w	water
exp	experimental		

REFERENCES

American Society of Heating, Refrigerating and Air-Conditioning Engineers, Inc. (2013). *ASHRAE Standard 34, Designation and safety classification of refrigerants*.

Cavallini, A., Censi, G., Del Col, D., Doretti, L., Matkovic, M., Rossetto, L., Zilio, C. (2006). Condensation in horizontal smooth tubes, a new heat transfer model for heat exchanger design. *Heat Transfer Eng., 27* (8), 31–38.

Churchill, S.W. (1977). Friction Factor Equations Spans All Fluid-Flow Regimes. *Chemical Engineering Journal, 84*, 91-92.

Davenport, C. J. (1983). Correlation for heat transfer and flow friction characteristics of louvered fin, *AIChE Symposium Series, 225*, 19-27.

Del Col, D., Azzolin, M., Bisetto, A., Bortolin, S. (2015). Frictional Pressure Drop during Two-Phase Flow of Pure Fluids and Mixtures in Small Diameter Channels. *Int. J. Chemical Reactor Eng., 13*(4), 493-502.

Del Col, D., Bortolato, M., Azzolin, M., Bortolin, S. (2015). Condensation heat transfer and two-phase frictional pressure drop in a single minichannel with R1234ze(E) and other refrigerants. *Int. J. Refrig., 50*, 87-103.

Del Col, D., Bortolin, S., Rossetto, L. (2013). Convective boiling inside a single circular microchannel, *Int. J. Heat and Mass Transf., 67*, 1231-1245.

Del Col, D., Cavallini, A., Da Riva, E., Mancin, S., Censi, G. (2010). Shell-and-Tube Minichannel Condenser for Low Refrigerant Charge. *Heat Transfer Engineering, 31*(6), 509-517.

García-Cascales, J.R., Illán-Gomez, F., Hidalgo-Mompeán, F., Ramírez-Rivera, F., Ramírez-Basalo, M.A. (2016). Performance comparison of an air/water heat pump using a minichannel coil as evaporator in replacement of a fin-and-tube heat exchanger. *International Journal of Refrigeration*, *74*, 560-575.

Illán-Gomez, F., García-Cascales, J.R., Hidalgo-Mompeán, F., Lopez-Belchi, A. (2017). Experimental assessment of the replacement of a conventional fin-and-tube condenser by a minichannel heat exchanger in an air/water chiller for residential air conditioning. *Energy and Buildings, 144*, 104-116.

Irudaya Raj, V. D. & Logesh, K. & Vasudevan, A. & Nishant, B. B. & Deepak, A. & Arvind, T. (2017). Experimental Investigation on Energy Saving Potential of Smart HVAC Unit. *International Journal of Ambient Energy*. 1-8.

Kim, N.-H., Byun, H.-W. (2013). Effect of inlet configuration on upward branching of two-phase refrigerant in a parallel flow heat exchanger. *International Journal of Refrigeration*, *36*(3). 1062–1077.

Kulkarni, T., Bullard, C.W., Cho, K. (2004). Header design tradeoffs in microchannel evaporators. *Applied Thermal Engineering*, *24*(5-6). 759-776.

Lazarek, G.M. & Black, S.H. (1982). Evaporative heat transfer, pressure and critical heat flux in small vertical tube with R113. *Int. J. Heat Mass Transf., 25*, pp. 945-960.

Lemmon, E.W., Huber, M.L., McLinden, M.O. (2013). NIST Standard Reference Database 23: Reference Fluid Thermodynamic and Transport Properties-REFPROP, Version 9.1, *National Institute of Standards and Technology, Standard Reference Data Program*, Gaithersburg.

Matkovic, M., Cavallini, A., Del Col, D., Rossetto, L. (2009). Experimental study on condensation heat transfer inside a single circular minichannel. *Int. J. Heat and Mass Transf., 52*, 2311–2323.

Mota-Babiloni, A., Navarro-Esbrí, J., Makhnatch, P., Molés, F. (2017). Refrigerant R32 as lower GWP working fluid in residential air conditioning systems in Europe and the USA. *Renewable and Sustainable Energy Reviews. 80*, 1031-1042.

Muzychka, Y. S. & Yovanovich, M. M. (2004). Laminar Forced Convection Heat Transfer in the Combined Entry Region of Non-Circular Ducts. *Journal of Heat Transfer-transactions of The Asme, 126*(1), 54-61.

Park, C. & Hrnjak, P. (2008). Experimental and numerical study on microchannel and round-tube condensers in a R410A residential air-conditioning system. *International Journal of Refrigeration-revue Internationale Du Froid, 31*(5). 822-831.

Rouhani, S.Z. (1978). Chapter 12: steady-state void fraction and pressure drop in water-cooled reactors. In: Ginoux, J.J. (Ed.), Two-Phase Flows and Heat Transfer with Application to Nuclear Reactor Design Problems. Hemisphere Pub. Corp., Washington, pp. 241–327.

Rouhani, S.Z., Axelsson, E. (1970). Calculation of void volume fraction in the subcooled and quality boiling regions. *Int. J. Heat Mass Transf*. 13, 383–393.

Threlkeld, J. L., Kuehn, T. H., Ramsey, J. W. *Thermal Environmental Engineering*. (1998). Prentice Hall.

Wang, C.-C., Chi, K.-Y., Chang, C.-J. (2000). Heat transfer and friction characteristics of plain fin-and-tube heat exchangers, part II: Correlation. *International Journal of Heat and Mass Transfer, 43*(15), 2693-2700.

ACKNOWLEDGEMENT

The authors acknowledge the support of the European project GEOTeCH (www.geotech-project.eu) which has received funding from the European Union's Horizon 2020 research and innovation program under grant agreement No. 656889.